Apoptotic β-cells induce macrophage reprogramming under diabetic conditions

Received for publication, June 21, 2018, and in revised form, September 6, 2018 Published, Papers in Press, September 13, 2018, DOI 10.1074/jbc.RA118.004565

Meliza G. Ward, Ge Li, and Mingming Hao[1]

From the Department of Biochemistry, Weill Medical College of Cornell University, New York, New York 10065

Edited by Jeffrey E. Pessin

Type 2 diabetes mellitus (T2DM) occurs when insulin-producing pancreatic β-cells fail to secrete sufficient insulin to compensate for insulin resistance. As T2DM progresses, apoptotic β-cells need to be removed by macrophages through efferocytosis that is anti-inflammatory by nature. Paradoxically, infiltrating macrophages are a main source of inflammatory cytokines that leads to T2DM. It is unclear how apoptotic β-cells impact macrophage function. We show under diabetic conditions, phagocytosis of apoptotic β-cells causes lysosomal permeabilization and generates reactive oxygen species that lead to inflammasome activation and cytokine secretion in macrophages. Efferocytosis-induced lipid accumulation transforms islet macrophages into foam cell–like outside the context of atherosclerosis. Our study suggests that whereas macrophages normally play a protective anti-inflammatory role, the increasing demand of clearing apoptotic cells may trigger them to undergo proinflammatory reprogramming as T2DM progresses. This shift in the balance between opposing macrophage inflammatory responses could contribute to chronic inflammation involved in metabolic diseases. Our study highlights the importance of preserving macrophage lysosomal function as a therapeutic intervention for diabetes progression.

Type 2 diabetes mellitus (T2DM)[2] is becoming a global epidemic. Growing recognition of chronic islet inflammation as a critical factor in the pathogenesis of T2DM opens up a new area in β-cell research. It highlights the importance of macrophages in islet biology (1). In healthy organs, apoptotic cells are rapidly cleared by phagocytic cells, making the presence of dead cells rare (2). The process of clearing apoptotic cells is termed efferocytosis, which involves engulfment of apoptotic cells by macrophages, followed by cell debris targeted to and degraded by digestive enzymes in the acidic lysosomes. Under normal conditions, efferocytosis reprograms macrophages toward an anti-inflammatory phenotype that results in resolution of inflammation (3).

Pancreatic β-cells specialize in the synthesis and release of insulin in response to glucose. Similar to that of lysosomes, the internal milieu of insulin granules creates an acidic environment maintained through ATPases and allows for the crystallization of insulin around zinc molecules (4). Unlike most materials, insulin crystals are notoriously slow to degrade in the lysosomes, shown by studies of the β-cells and liver cells as well as *in vitro* processing by lysosomal proteases (5). A resting mouse β-cell has roughly 10,000 insulin granules, each may contain as many as 20,000 insulin crystals (6). Thus, when presented with an increased demand for β-cell efferocytosis (phagocytosis of apoptotic β-cells) in T2DM, macrophages must deal with the accumulation of insulin crystals that are not readily degraded by the lysosomes. To date there has been no study that addresses the impact of long-lived insulin crystals on macrophage function.

After engulfment, pathogenic crystals (monosodium urate, calcium pyrophosphate dihydrate, cholesterol, and cysteine crystals) permeabilize lysosomal membrane and activate the NLRP3 inflammasomes (7–9). The pathogenicity of a crystal is influenced by its size and shape, as not all crystal particles activate the inflammasome (10). In addition to crystals, substances that are generally thought to be inert can effect lysosomal dysfunction (11). Whether the insulin crystal can behave as a pathogenic crystal or lysosomal antagonist prompted us to test the idea that β-cell efferocytosis may lead to lysosomal defects due to accumulation of insulin crystals in macrophages.

Chronic islet inflammation contributes to the pathogenesis of T2DM (1). Pancreatic islets from diabetic patients have increased macrophage infiltration (12). The proinflammatory cytokine interleukin-1β (IL-1β) is a major contributor to islet inflammation and T2DM by reducing β-cell function and promoting β-cell apoptosis (13). IL-1β secretion requires the activation of NLRP3 inflammasomes, as Nlrp3 knockout mice fed a high-fat diet showed reduced islet IL-1β protein expression and β-cell death compared with WT mice (14). However, the mechanisms of NLRP3 inflammasome activation in infiltrating macrophages are not fully understood (15). Endocannabinoids and human islet amyloid polypeptides are thus far the only identified activators of the NLRP3 inflammasomes in infiltrating islet macrophages (16, 17). In this study, we conducted *in vitro* experiments to show insulin crystals from β-cell efferocytosis can cause inflammasome activation and release of IL-1β

This work was supported by Cornell University, Weill Cornell Graduate School of Medical Sciences. The authors declare that they have no conflicts of interest with the contents of this article.

This article contains Figs. S1–S7.

[1] To whom correspondence should be addressed: 1300 York Ave., New York, NY 10065. Tel.: 646-962-9817; Fax: 646-962-0519; E-mail: mhao@med.cornell.edu.

[2] The abbreviations used are: T2DM, type 2 diabetes mellitus; IL-1β, interleukin-1β; BMMs, bone marrow-derived primary macrophages; apMIN6, apoptotic MIN6; CtB, cholera toxin subunit B; HG, high glucose; HGP, high glucose with palmitate; LPS, lipopolysaccharide; ROS, reactive oxygen species; NAC, *N*-acetylcysteine; TFEB, transcription factor EB; PI, propidium iodide; H_2DFFDA, 5-(and-6)-carboxy-2′,7′-dihydrofluorescein diacetate; DMEM, Dulbecco's modified Eagle's medium; STZ, streptozotocin; ANOVA, analysis of variance.

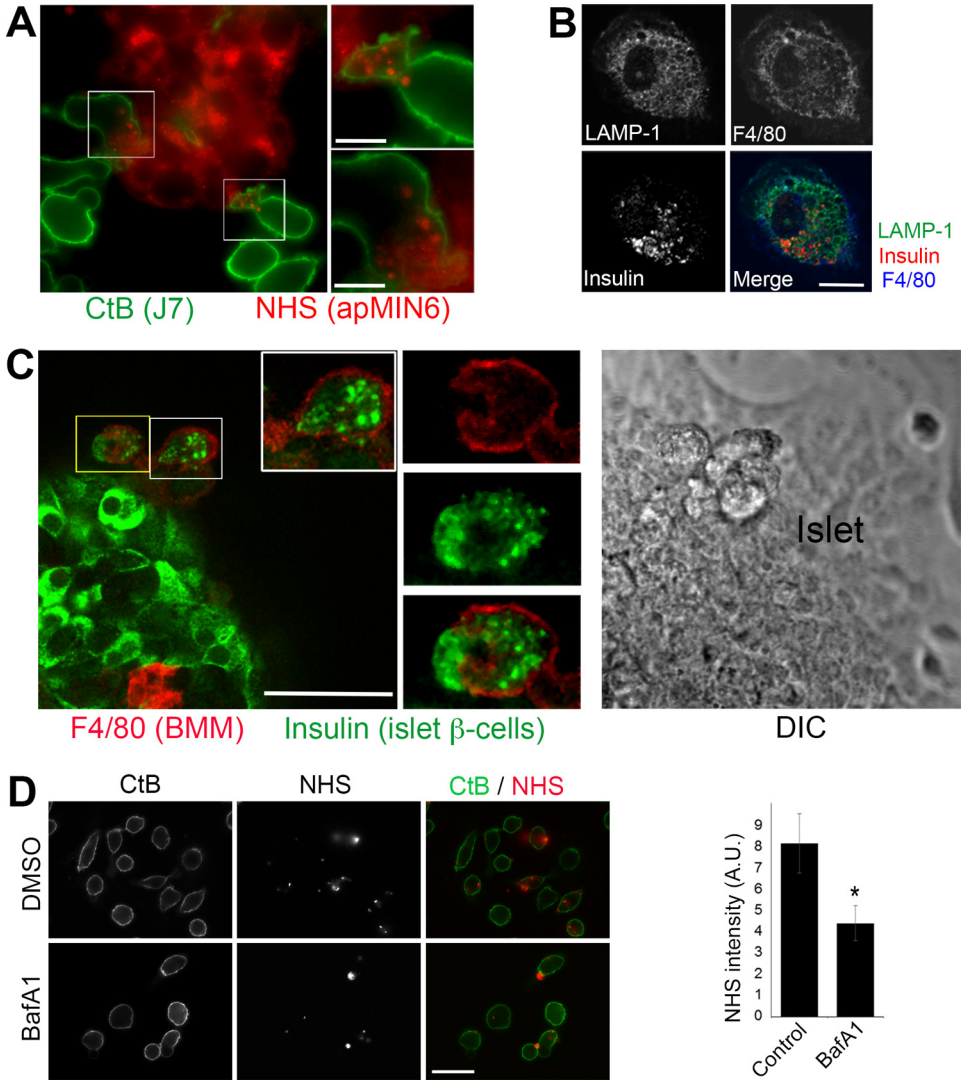

Figure 1. Experimental models for studying β-cell efferocytosis *in vitro*. *A*, co-culture of J7 with apMIN6. apMIN6 cells were labeled with NHS (*red*) before incubation with J7 cells overnight, followed by CtB labeling (*green*) and wide-field microscopy. *B*, primary islet macrophages from STZ-treated apoptotic islets. Single islets isolated from STZ-treated mice were seeded individually in imaging dishes and stained with F4/80, insulin, and LAMP-1 antibodies. Shown here is a confocal image of an islet macrophage that migrated out of the islet. *C*, interaction of BMMs with apoptotic islets. Isolated islets were cultured for 2 weeks to induce apoptosis before BMMs were added for 24 h. The co-culture was stained with F4/80 and insulin antibodies, and imaged by confocal microscopy. The differential interference contrast (*DIC*) panel shows the imaged portion of the islet. *D*, verification that NHS-labeled apoptotic bodies were phagocytosed by macrophages. Floating apMIN6 cells were labeled with NHS (*red*) before incubation with attached J7 cells for 2 h with or without bafilomycin A1 (*BafA1*) followed by extensive rinsing, and imaged by wide-field microscopy. CtB (*green*) was used to label J7 plasma membrane. NHS fluorescence inside CtB was quantified from 60 cells. *, $p < 0.05$. *A.U.*, arbitrary units. *Scale bars*: 10 μm (*A* and *B*), 50 μm (*C* and *D*).

from macrophages, thus acting as a previously unrecognized cause of islet inflammation *in vitro*.

Results

In vitro and in vivo experimental models for studying β-cell efferocytosis

To study β-cell efferocytosis, we created an *in vitro* system using bone marrow-derived primary macrophages (BMMs) or J774a.1 macrophage-like cells (J7) incubated with UV-induced apoptotic MIN6 cultured β-cells (apMIN6) or apoptotic-isolated islets. Presented in Fig. 1, *A–C* are images demonstrating the *in vitro* experimental systems specifically set up for this study. Efferocytosis was carried out by overnight incubation of BMMs or J7 cells with apMIN6 cells, where the J7 cells were labeled with Alexa 488-cholera toxin subunit B (CtB) and apMIN6 cells were labeled with succinimidyl esters (NHS) of Alexa Fluor-546 (18). J7 cells (*green*) were observed to be engulfing pieces of apMIN6 cells (*red*) during efferocytosis (Fig. 1*A*, enlarged cells to the right). To study primary islet macrophages derived *in vivo*, we induced islet cell death *in vivo* by injecting mice with five low doses of streptozotocin 2 weeks prior to islet isolation (19). We used F4/80, an extensively used surface marker for mouse macrophages (20), to identify macrophages. Because islet macrophages were few in number (12, 21) and antibody penetration was severely limited for an intact islet, cells labeled with F4/80 were rarely found inside an islet. Therefore, we focused on islet macrophages that migrated out of an islet during *in vitro* culturing (Fig. 1*B*, the islet is not shown), similar to the examples shown in Fig. S1, *A* and *B*. We used F4/80 (*blue*) to detect macrophages, insulin (*red*) to verify that

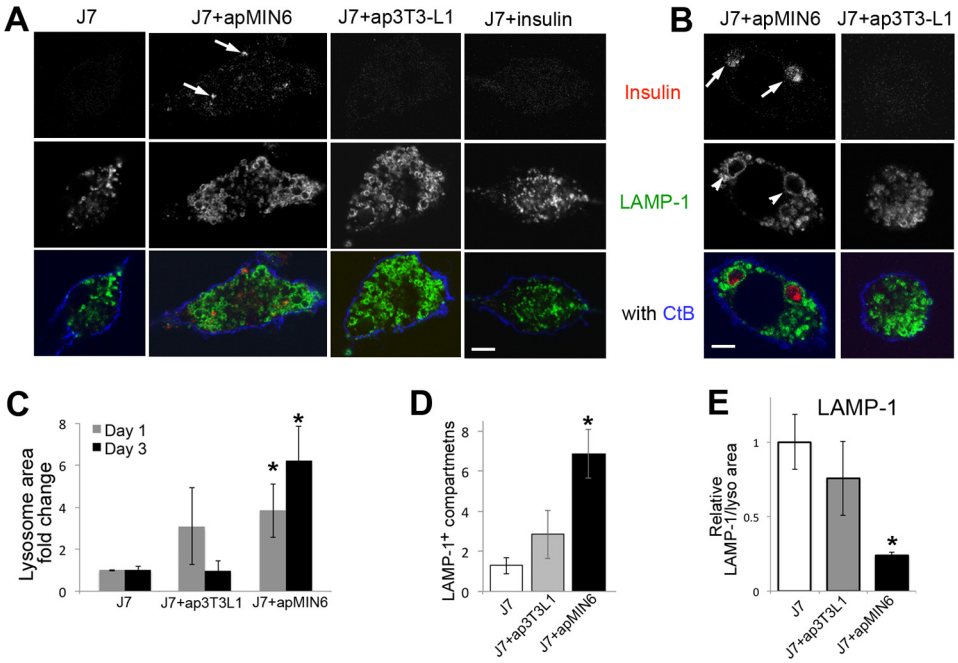

Figure 2. Phagocytosis of apMIN6 cells leads to insulin accumulation and enlarged lysosomes. *A* and *B,* incubation with apMIN6, but not ap3T3-L1 or monomeric insulin, induced insulin accumulation, and lysosome swelling. One day after efferocytosis, insulin was detected in LAMP-1 positive lysosomes indicated by the *arrows* (*A*). By day 3, enlarged lysosomes (*arrowheads*) were found in J7 cells incubated with apMIN6 (*B*) by confocal microscopy. *Scale bars*, 5 μm. *C,* two-dimensional lysosome area was measured by manually tracing the lysosomes outlined by LAMP-1. *D,* lysosome outlines were determined by LAMP-1, and those with a diameter greater than 2 μm were counted. *E,* LAMP-1 fluorescence intensity was measured and normalized to lysosome area. C–*E,* data are presented as fold-change relative to J7 cells alone. $n = 48$ lysosomes from 9 cells. *, $p < 0.05$ *versus* J7 alone.

efferocytosis had taken place, and LAMP-1 (*green*) to identify the lysosomes as the compartment in which ingested insulin accumulated. To induce islet cell death *in vitro*, islets were kept in culture for 2 weeks followed by incubation with BMMs (Fig. 1*C*). Here we again observed insulin-positive cell debris (*green*) inside F4/80-positive BMMs (*red*). We also used flow cytometry to show insulin accumulation in J7 cells after phagocytosis of apMIN6 cells (Fig. S1*C*). Finally, we included bafilomycin A1, a partial inhibitor of phagocytosis (22), during the incubation of J7 cells with apMIN6 cells to make sure that the NHS-positive cell debris associated with macrophages truly reflected phagocytosed material *versus* nonspecific sticking to macrophage cell surfaces (Fig. 1*D*). Bafilomycin treatment did not affect cell viability (data not shown).

Phagocytosis of apMIN6 cells leads to insulin accumulation and enlarged lysosomes

Phagocytosis of apMIN6 cells led to insulin staining in LAMP1-postive lysosomes in J7 cells 1 day after efferocytosis (Fig. 2*A*, *arrows*). We used apoptotic 3T3-L1 cells (ap3T3-L1) as a control for efferocytosis of noninsulin cells. Incubation of J7 cells with monomeric insulin in solution did not cause accumulation of insulin (Fig. 2*A*, *J7+insulin*), indicating the insulin detected in the J7 lysosomes came from phagocytosis of apMIN6 cells. After removing apMIN6 cells and waiting for 3 days, insulin from β-cell efferocytosis remained in J7 lysosomes (Fig. 2*B*, *arrows*) and caused marked lysosomal swelling (Fig. 2*B*, *arrowheads*, Fig. S2*A*). This phenomenon was not observed in J7 cells 3 days after phagocytosis of ap3T3-L1 cells (Fig. 2*B*) or incubation with monomeric insulin for 3 days (Fig. S2*B*). Lysosome size increased in J7 cells after a 1-day incubation with either apMIN6 or ap3T3-L1 cells (Fig. 2*C*, *gray bars*) in response to efferocytosis. However, J7 cells incubated with apMIN6 cells but not with ap3T3-L1 cells still had enlarged lysosomes 3 days (Fig. 2*C*, *black bars*) or even 7 days (not shown) after removal of apMIN6 cells. Quantified by another method, J7 cells incubated with apMIN6 cells had significantly more LAMP-1 positive compartments that were greater than 2 μm in diameter (Fig. 2*D*, *black*). The comparison with ap3T3-L1 cells (Fig. 2*D*, *gray*) suggested insulin accumulation as the underlying cause for the change in lysosomal morphology. As a marker for lysosome biogenesis, we measured total LAMP-1 expression. When normalized to the lysosome area, there was a deficit in LAMP-1 as a result of β-cell efferocytosis (Fig. 2*E*). To see if enlarged lysosomes were observed in macrophages from a diabetes mouse model, we isolated pancreatic islets from wildtype (WT) and db/db diabetic mice, and stained dissociated islet cells with F4/80 to identify macrophages and LAMP1 to label lysosomes. A db/db macrophage shown in Fig. S2*D* displayed enlarged lysosomes (*yellow arrowheads*) compared with that of WT (Fig. S2*C*). The histogram distribution analysis of LAMP1 structures (Fig. S2*E*) within the expected size range (23) show that whereas the majority of the lysosomes (<0.5 μm^2, Fig. S2*F*) were similar in size between WT and db/db, the number of lysosomes that were >0.5 μm^2 (Fig. S2*G*) was significantly higher in db/db macrophages. These results show that the dynamic regulation of lysosomal biogenesis that normally accompanied efferocytosis was disrupted in cells with insulin accumulation, which was most likely contributed by the prolonged presence of slowly degradable insulin crystals (4, 5, 24).

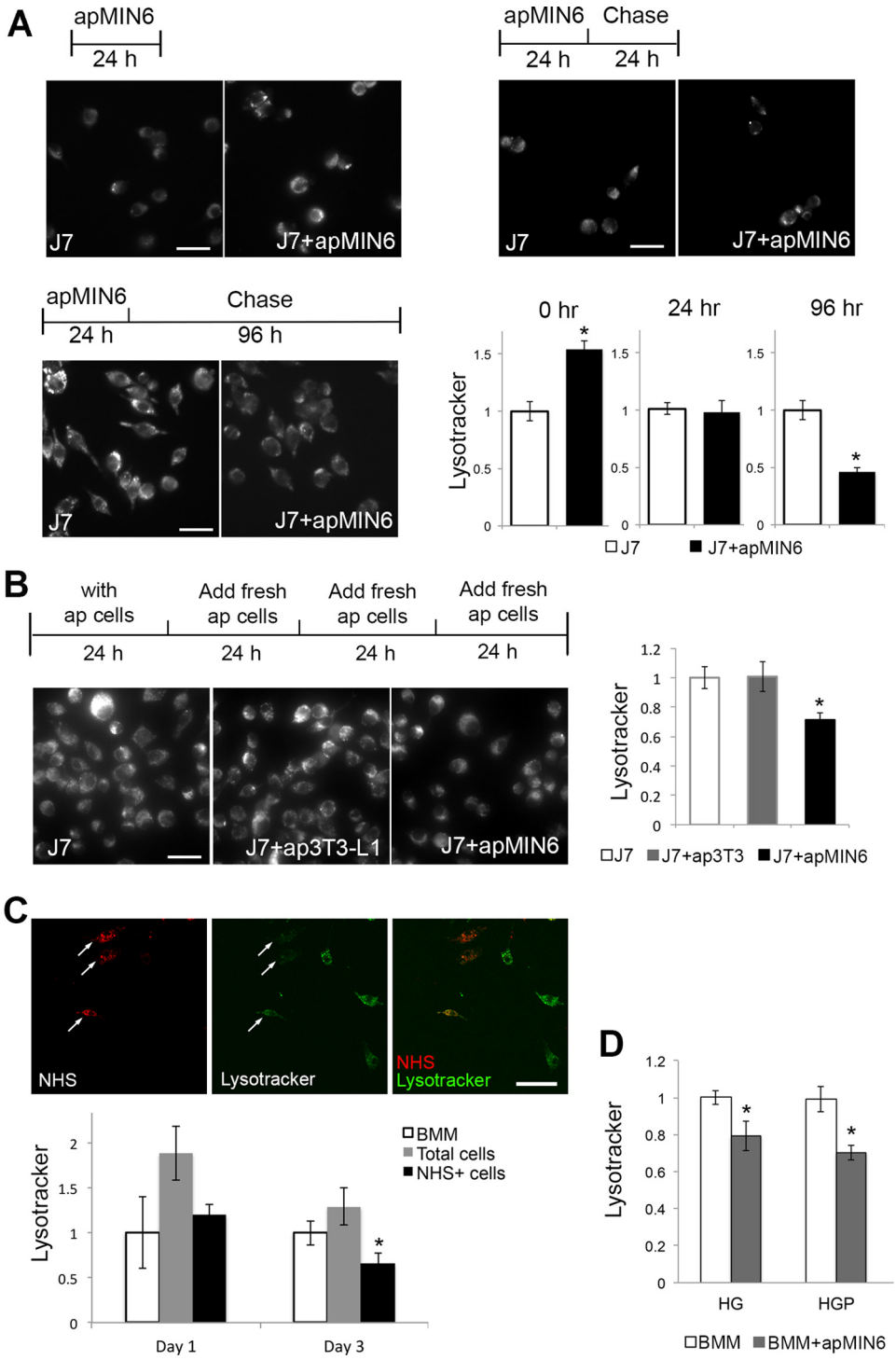

Figure 3. LysoTracker staining was decreased by phagocytosis of apMIN6 cells. *A,* J7 cells were incubated with apMIN6 for 24 h, chased for various lengths of time, labeled with LysoTracker and imaged by wide-field microscopy. LysoTracker fluorescence per cell from 16 imaging fields was quantified. *B,* J7 cells were pulsed with fresh apMIN6 every 24 h for 96 h before being labeled by LysoTracker, with apoptotic 3T3-L1 (*ap3T3*) used as a control for general efferocytosis of noninsulin containing cells. $n = 12$ imaging fields. *C,* BMMs were incubated with NHS-labeled apMIN6 for 24 h and chased for 3 days before LysoTracker fluorescence was measured from all cells (*gray bars*) or NHS-positive cells (*black bars*). *Arrows* point to NHS-positive BMMs indicating efferocytosis. At least 20 cells were used for each condition. *D,* BMMs were incubated with apMIN6 for 24 h and chased for 3 days in HG or HGP medium before LysoTracker fluorescence was measured from all cells. $n = 9$ imaging fields. All measurement was normalized to that obtained in J7 or BMMs alone (control). *, $p < 0.05$ *versus* control. *Scale bars*, 50 μm.

Phagocytosis of apMIN6 cells induces lysosomal dysfunction

Because phagocytosis of apMIN6 cells induced morphological changes in macrophage lysosomes, we examined the consequences of β-cell efferocytosis on lysosomal function. LysoTracker concentrates in acidic organelles and is a general marker for lysosomal function (25). We performed a time course study in which J7 cells were incubated with apMIN6 cells and then labeled with LysoTracker (Fig. 3*A*). LysoTracker

staining first increased immediately after efferocytosis (0 h chase), consistent with up-regulation of lysosomal biogenesis that may decrease lysosomal pH to enhance the activity of lysosomal enzymes. The level of LysoTracker returned to normal 24 h after efferocytosis and continued to decrease until it was only half of that in the control cells 96 h after efferocytosis. When J7 cells were continuously pulsed with a fresh supply of apMIN6 cells every 24 h to mimic the continuous presence of apoptotic β-cells *in vivo*, LysoTracker staining was still significantly decreased after 96 h, which was not the case with ap3T3-L1 cells (Fig. 3*B*).

Using NHS-labeled apMIN6 cells, there was less LysoTracker accumulation in BMMs that actively phagocytosed NHS-apMIN6 cells (Fig. 3*C*, *arrows*) compared with NHS-negative BMMs. When LysoTracker staining was quantified in NHS-positive BMMs, a significant decrease was detected compared with BMMs alone (Fig. 3*C*, *Day 3*). The decrease in LysoTracker fluorescence was not simply due to an exclusion of LysoTracker by insulin accumulation, because dextran concentrated and co-existed with insulin in the enlarged lysosomes in both J7 cells and BMMs (Fig. S2*A*). To study how elevated glucose and excess fatty acids affect macrophage function, we exposed BMMs to high glucose (HG) or high glucose with palmitate (HGP). Supraphysiological concentration of glucose (30 mM) was used as HG because it is a widely used tool to produce glucose-induced cellular dysfunction *in vitro*. We acknowledge that this is purely an *in vitro* experimental system. There was no difference in LysoTracker for control *versus* HG-treated or control *versus* apMIN6-exposed BMMs. When BMMs was treated with HG or HGP, LysoTracker staining was modestly decreased with statistical significance in BMMs exposed to apMIN6 cells compared with BMMs alone, quantified from all the cells (Fig. 3*D*). This result suggested that additional metabolic stress could exacerbate lysosomal defects. Because HG and HGP seemed to affect lysosomal function to a similar degree, we focused on the HG treatment.

Phagocytosis of apMIN6 cells induces functional defects in lysosomes

An increase in lysosomal pH could contribute to the reduced intensity of the acidotropic LysoTracker (26). We used fluorescence ratio imaging of lysosomes containing endocytosed fluorescein-rhodamine-dextran (27) to determine whether efferocytosis altered lysosomal pH. Fluorescein fluorescence increases as pH increases, whereas rhodamine fluorescence is pH independent, thus rendering the fluorescein/rhodamine ratio pH-dependent (Fig. S3). BMMs and BMMs exposed to apMIN6 cells cultured in normal medium did not show significant difference in lysosomal pH (data not shown). When cultured in HG medium, BMMs + apMIN6 showed larger lysosomes with higher fluorescein/rhodamine ratio, indicating higher lysosomal pH (Fig. 4*A*). When individual lysosomes were quantified, there were more lysosomes with higher pH values (Fig. 4*B*). Because lysosomes with insulin accumulation were larger, we measured lysosomal pH according to the size of the lysosomes. Interestingly, all lysosomes have reduced acidification after β-cell efferocytosis (Fig. 4*C*), suggesting a general defect in the lysosomal system.

Because increased pH can greatly compromise the proteolytic power of lysosomes, we next examined if reduced lysosomal acidification due to β-cell efferocytosis could lead to inefficient degradation of lysosomal contents. We took advantage of a fluorogenic substrate for proteases, DQ-ovalbumin. Hydrolysis of DQ-ovalbumin by lysosomal proteases relieved the self-quenched BODIPY FL dyes, resulting in increased fluorescence intensity (28) and formation of excimers that can be visualized using a red emission long pass filter (Fig. 4*D*, *panel ii*). There was a noticeable decrease in the number of excimer puncta observed in cells exposed to apMIN6 cells (Fig. 4*D*, *panel iv versus panel ii*). When quantified, total fluorescence intensity was reduced from both DQ channels (Fig. 4*E*), suggesting a diminished proteolytic capacity of the lysosomes.

Lysosome permeabilization in phagocytic macrophages exposed to high glucose

The reduced LysoTracker staining after β-cell efferocytosis could be due to either a rise in lysosomal pH or leakage in lysosomal membrane. To see if there was lysosomal leakage, we used pH-independent, lysine-fixable dextran compatible with co-staining with other markers. Although the morphology of the lysosomes was altered in both J7 cells (Fig. 5*A*) and BMMs (Fig. 5*B*, Fig. S2*A*), dextran was confined to the LAMP-1 positive compartments and co-existed with insulin aggregates (Fig. 5*A*, *arrowheads*). Two of the enlarged lysosomes in a BMM are shown in Fig. 5*B* outlined by LAMP-1 (*cyan*) with dextran (*red*) and insulin (*green*) inside. These results show that although insulin aggregates caused lysosome swelling, they were not as potent as other pathogenic crystalline particulates in inducing lysosome permeabilization (7–9).

We next imaged dextran-loaded BMMs in high glucose culture (HG-BMMs) to test if additional cell stress would induce lysosome permeabilization. Dextran remained in distinct puncta after efferocytosis in control BMMs, indicating intact lysosomes (Fig. 5*C*, *yellow box*). When HG-BMMs were exposed to apMIN6, less dextran was found in enlarged insulin-positive lysosomes (Fig. 5*D*, *arrowhead*). More importantly, dextran appeared as additional diffuse staining in the cytoplasm, indicating leakage from lysosomes (Fig. 5*D*, *yellow box*). Even at single confocal planes, dextran was present in the cytoplasm (Fig. S4*B*, *yellow box*). HG treatment alone did not induce either enlarged lysosomes or lysosomal leakage (Fig. S4*C*). We quantified the distribution of dextran in control and HG-BMMs after efferocytosis (Fig. 5, *C* and *D*). Compared with BMMs, HG-BMMs had a 21.4 ± 4% decrease in the ratio of dextran intensity in the lysosomes (punctate structures) to total dextran intensity ($n = 8$ imaging fields per condition). We next performed live-cell imaging of BMMs co-cultured with apoptotic islets to mimic the *in vivo* interaction of macrophages with islets. This would also rule out the possibility that fixation and permeabilization was the cause for the dextran observed in the cytoplasm, even when lysine-fixable dextran was used. Shown in Fig. 5, *E* and *F*, are two regions of the same islet co-cultured with HG-BMMs prelabeled with dextran. BMMs situated outside the islet (Fig. 5*E*, *box 1*) had small punctate dextran staining, similar to BMMs cultured alone (Fig. S5*A*). For BMMs in contact with the islet cells (Fig. 5*F*, *box 2*), either on the cover-

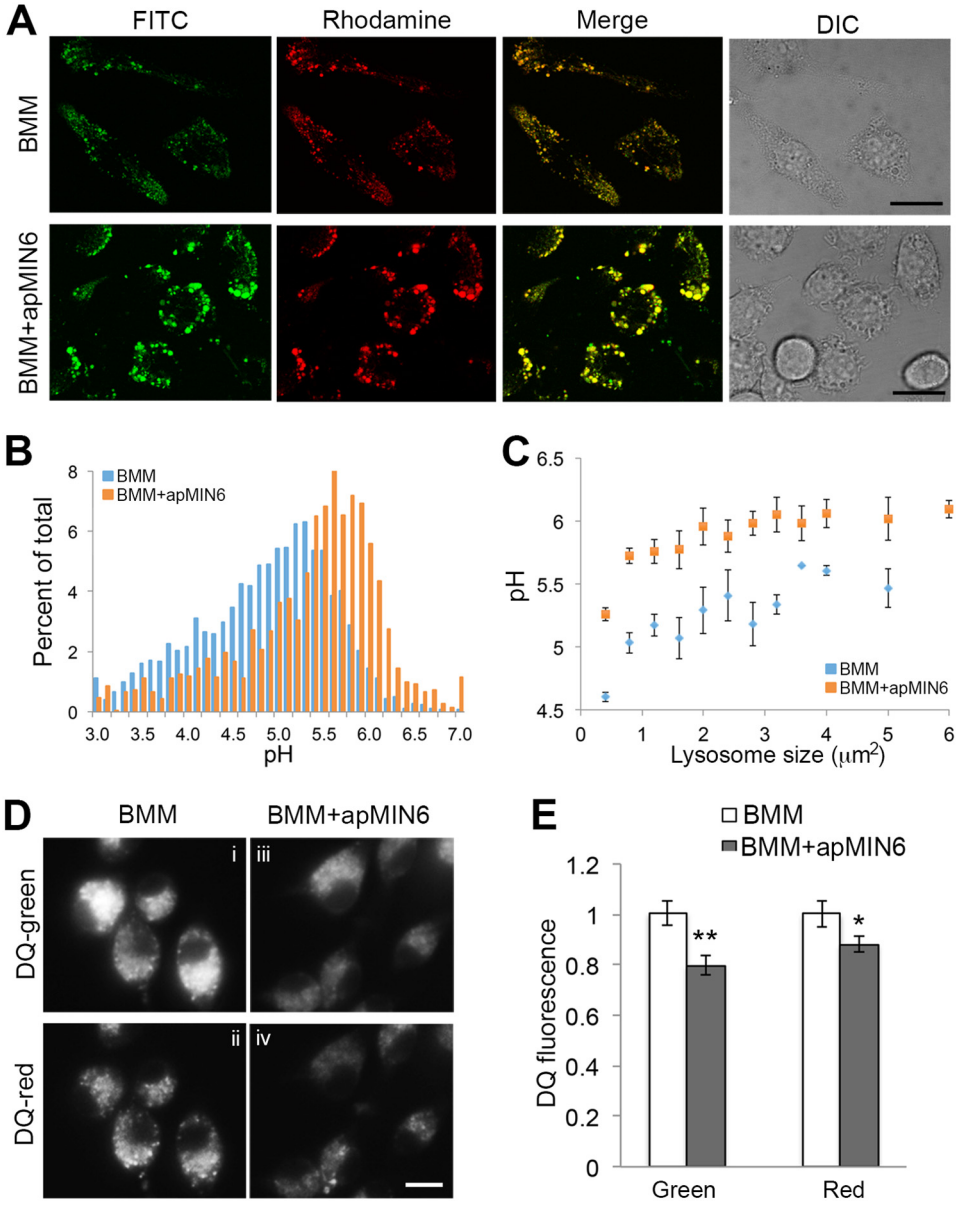

Figure 4. Lysosomal dysfunction as a result of phagocytosis of apMIN6. *A–C*, lysosomal pH was measured using FITC-rhodamine dextran in living BMMs by confocal microscopy (*A*), and quantified by the ratio of FITC (*green*) to rhodamine (*red*) fluorescence in each individual lysosome (*B* and *C*). *B*, histogram of lysosomal pH values from BMMs alone and BMMs exposed to apMIN6. *C*, lysosomes were pooled and an average of their pH values are presented as a function of lysosome sizes. *D* and *E*, the proteolytic capacity of the lysosomes was measured using a fluorogenic substrate for lysosomal proteases, DQ-ovalbumin (*DQ*), whose green fluorescence increased dramatically upon hydrolysis by proteases. Concentrated DQ fragments gave rise to red fluorescence emission. BMMs were treated with HG prior to loading with DQ. DQ fluorescence per cell was quantified from 12 imaging fields. *, $p < 0.05$; **, $p < 0.01$. *Scale bars*, 20 μm.

slip plane (Fig. 5*F*) or inside the islet away from the coverslip (Fig. S5*B*), several BMMs showed enlarged lysosomes (Fig. 5*F*, *white arrowheads*) along with the presence of dextran in the cytoplasm (Fig. 5*F*, *yellow arrows*). It suggested that glucose-induced cell stress resulted in the weakening of the lysosomal membrane, thus enabling insulin aggregates to permeabilize the lysosomal membrane. If this were true, we should see less dextran in a portion of the lysosomes in phagocytic HG-BMMs due to insulin-induced permeabilization. When cultured in normal medium, there was a slight right shift in the dextran intensity from phagocytic BMMs compared with BMMs alone (Fig. 5*G*). On the other hand, when BMMs were pretreated with HG, there was a significant left shift in the dextran intensity in phagocytic BMMs, indicating reduced dextran in the permeabilized lysosomes (Fig. 5*H*).

High glucose induces pro-inflammatory responses from phagocytic BMMs

Lysosome permeabilization by pathogenic crystals results in NLRP3-inflammasome activation and IL-1β secretion. To see if efferocytosis-induced lysosomal leakage would promote macrophage inflammation, we show altered gene expression of TNFα, IL-18, and IL-10 (Fig. S6*A*). For control BMMs, β-cell efferocytosis had little effect on IL-1β release, most likely due to the very low levels of cytokine production in unprimed macrophages (3). When BMMs were primed with bacterial lipopoly-

saccharide (LPS) to stimulate cytokine production, an increase in IL-1β secretion was detected. Interestingly, β-cell efferocytosis significantly decreased LPS-stimulated IL-1β secretion (Fig. 6*A*), exhibiting an anti-inflammatory response usually elicited by efferocytosis. Similar results showed that efferocytosis of apoptotic neutrophils by BMMs inhibited cytokine release (3). If BMMs were first cultured in HG, efferocytosis of MIN6 but not 3T3-L1 significantly increased IL-1β secretion (Fig. 6*B*, Fig. S6*B*). HG treatment did not further increase IL-1β secretion from LPS-treated samples (208 ± 36 *versus* 196 ± 41 pg/ml). The absolute concentrations of secreted IL-1β are shown in Fig. S6, *C* and *D*. Please note the physiological effect of IL-1β secretion cannot be evaluated based on the concentrations of IL-1β collected in solution *in vitro*, because *in vitro*

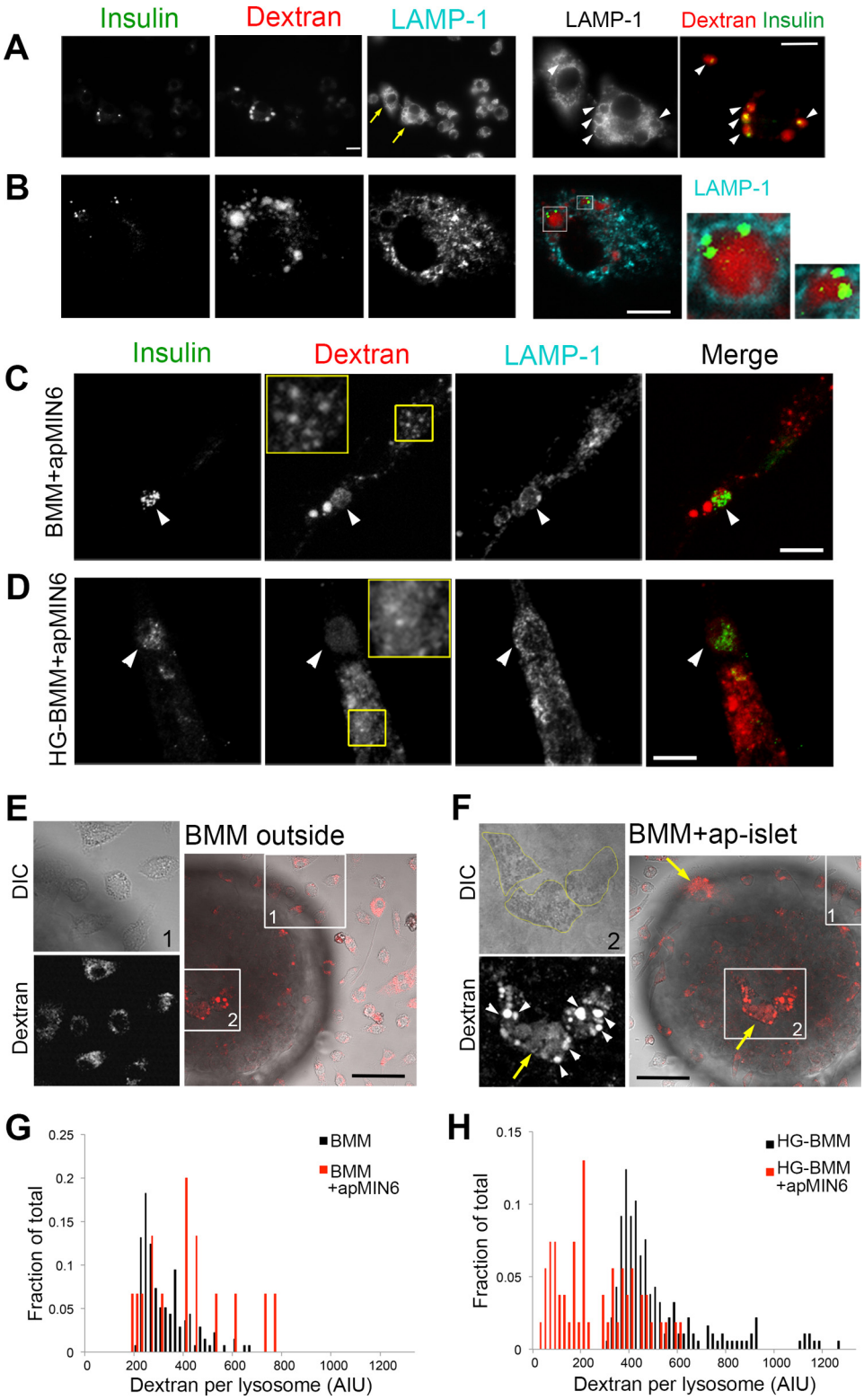

IL-1β secretion is measured during a fixed time period in an arbitrary volume. Even when *in vivo* circulating IL-1β is low, local concentration at the interface between islet macrophages and islet β-cells could be high enough to result in a significant effect, especially from continuous exposure. For example, it is shown that the IL-1 receptor is expressed at a particularly high level in the islet β-cells, which can respond to low levels of IL-1β to induce hyperinsulinemia and proinflammatory responses during prediabetes (29, 30). Although HG treatment alone did not induce IL-1β secretion (Fig. 6*B*), it promoted *Il1b* gene expression (Fig. 6*C*), consistent with the finding that the mRNA and protein expression of major inflammasome components NLRP3, caspase-1, and IL-1 were up-regulated by high glucose treatment (31). These results suggested that high glucose and β-cell efferocytosis together were sufficient to trigger IL-1β release.

IL-1β processing and release from macrophages depend on the NLRP3-inflammasome, whose activation requires the assembly of the proteolytic complex containing active caspase-1. To directly examine inflammasome activation, we used a fluorescent probe (FAM-YVAD-FMK FLICA) to detect specifically the activated caspase-1 enzyme (Fig. 6, *D–G*). Upon inflammasome assembly, active caspase-1 translocated to punctate "specks" in HG-BMMs (Fig. 6*D*, *arrows*), suggesting NLRP3-inflammasome activation (32). Although the total cell-associated fluorescence increased slightly (Fig. 6*E*), there was a significant increase in the number of specks from HG-BMMs (Fig. 6*F*). When NHS-labeled apMIN6 cells were used, we detected phagocytosed NHS within the specks that contained active caspase-1 (Fig. 6*G*) in 64.6 ± 2.1% of the cells ($n = 194$), consistent with the finding that inflammasome activation can lead to colocalization between inflammasomes and autophagosomes (33). The high degree of colocalization between FLICA and NHS was not an artifact of signal crossover, as shown in Fig. S6*E*.

Many of the known mechanisms for NLRP3-inflammasome activation converge in the production of reactive oxygen species (ROS), which is also a requisite for inflammasome activation (34). Using NHS to indicate apMIN6 cell fragments, we show that phagocytic HG-BMMs displayed significantly higher intensity of carboxy-H_2DFFDA, a fluorescent probe for ROS (35), than cells with less NHS (Fig. 6*H*, *arrows*). For control BMMs, β-cell efferocytosis induced ROS production; when BMMs were pretreated with HG, β-cell efferocytosis caused a dramatic increase in ROS production (Fig. 6*I*). Finally, when cells were treated with trehalose, a disaccharide that induces lysosome biogenesis (36), or the antioxidant *N*-acetylcysteine (NAC), IL-1β secretion was significantly reduced (Fig. 6*J*).

HG-BMMs undergo foam cell–like transformation after β-cell efferocytosis

Compared with BMMs alone, β-cell efferocytosis increased free cholesterol (labeled by filipin, Fig. 7*A*) and neutral lipids (labeled by LipidTOX, Fig. 7*B*), as quantified in Fig. 7*C*. However, it did not induce lipid droplet formation (no puncta in Fig. 7*B*). HG treatment induced the formation of a massive number of lipid droplets in BMMs after β-cell efferocytosis (Fig. 7, *D* and *E*). This result suggested that when high glucose was present, macrophages accumulated lipids and took on foam cell characteristics as a consequence of clearing apoptotic β-cells. We next verified that the increased LipidTOX staining was detected in islet macrophages. When apoptotic islets containing native islet macrophages cultured in HG were imaged, there were cells that stood out with substantial amounts of lipid droplets labeled by LipidTOX. They were much larger than the majority of islet cells, most of which were β-cells (Fig. 7*F*). This was observed in 17 of 19 LipidTOX-positive cells. The number and size of these lipid-laden cells were consistent with them being macrophages (12, 21), although it is possible that they are not. Because LipidTOX labeling was not compatible with antibody staining, we identified islet macrophages by F4/80 in separate images, which showed that F4/80-positive islet macrophages were indeed larger than their surrounding cells (Fig. 7*G*) in all the islets stained with F4/80 ($n = 5$). The islet macrophages were also readily distinguishable in the DIC images (Fig. 7, *F* and *G*, Fig. S7), likely due to their lipid accumulation.

Phagocytosis of apMIN6 cells induces cellular characteristics of inflammation

As we examined through hundreds of images of phagocytic BMMs, we observed that β-cell efferocytosis resulted in dramatically more BMMs that were multinucleated (Fig. 8*A*, *arrows*) and enlarged in size (Figs. 5, *A* and *F*, 6*D*, and 8*A*). The multinuclear morphology was specific to phagocytosis of insulin-containing apMIN6 cells, as it did not occur with ap3T3-L1 cells (Fig. 8*B*). Interestingly, the lipid-laden cells after β-cell efferocytosis were also more likely to be multinuclear (Fig. 8*C*). All LipidTOX-labeled cells that were multinuclear had distinct lipid droplets ($n = 92$ cells examined). Macrophages become multinucleated in response to crystals and when poorly degradable materials are present (37). It is a hallmark of chronic inflammation (38, 39). Furthermore, many of these BMMs no

Figure 5. High glucose induces lysosomal permeabilization in phagocytic macrophages. *A* and *B,* dextran and insulin aggregates co-exist in intact lysosomes. J7 cells (*A*) or BMMs (*B*) were loaded with lysine-fixable rhodamine dextran (*red*) after phagocytosis of apMIN6 cells, fixed, and labeled with insulin (*green*) and LAMP-1 (*cyan*) antibodies before being imaged by wide-field (*A*) and confocal (*B*) microscopy. The *yellow arrows* in *A* show two cells with insulin aggregates in enlarged lysosomes filled with dextran (*arrowheads*). The two cells are expanded in the *bottom panels* in *A*. Single plane images are shown in *B*. Two lysosomes are expanded to the *right*, which show co-existence of dextran and insulin. *C* and *D,* BMMs were incubated with apMIN6 cells and cultured in either normal medium (*C*, BMMs+apMIN6) or high glucose medium for 3 days (*D*, HG-BMMs+apMIN6). They were then loaded with lysine-fixable rhodamine-dextran and labeled with insulin and LAMP-1 antibodies. Shown here are summation projection images by confocal microscopy. The *yellow boxes* show a region of the cell in which the dextran shows punctate staining in the lysosomes (*C*) or additional diffuse staining in the cytoplasm (*D*). The merged images show insulin in *green* and dextran in *red*. *Scale bar*, 10 μm (*A–D*). *E* and *F,* HG-BMMs loaded with rhodamine-dextran were added to apoptotic islets and imaged live by confocal microscopy. Images in *E* and *F* focused on the BMMs that were outside (*box 1*) and inside (*box 2*) the same islet, respectively. *White arrowheads* show enlarged lysosomes and *yellow arrows* show diffuse dextran in the cytoplasm (*F*). *Scale bars*, 50 μm. *G* and *H,* quantification of dextran intensity in lysosomes of BMMs (*G*) or HG-BMMs (*H*) with or without phagocytosis of apMIN6 cells. Lysosomes of all cells under the same condition were pooled from one experiment; the results are representative of three experiments.

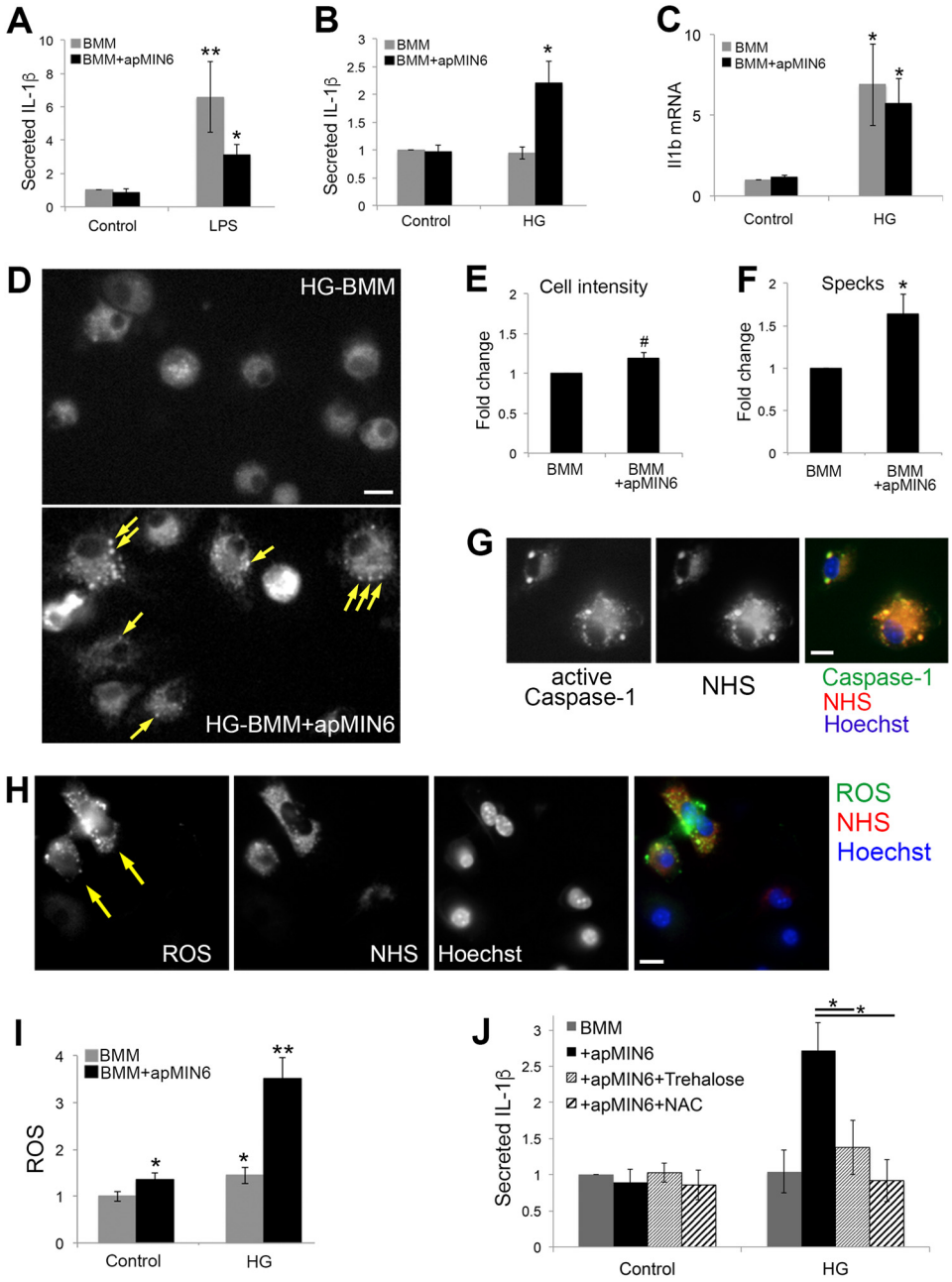

Figure 6. ROS and inflammation induced by β-cell efferocytosis and high glucose. *A–C*, BMMs kept in control (*A*) or HG (*B* and *C*) medium were cultured alone or overnight with apMIN6, and incubated for another 24 h with LPS (*A*) or in HG (*B* and *C*). *A* and *B*, medium was collected for ELISA of secreted IL-1β. *C*, expression of *Il1b* was measured by quantitative RT-PCR. **, $p < 0.01$ by Mann-Whitney Rank Sum Test; *, $p < 0.05$ by Student's *t* test. *D–G*, caspase-1 activation was visualized using FAM-FLICA. *D*, HG-BMMs with or without apMIN6 efferocytosis were labeled with FAM-FLICA and imaged by wide-field microscopy. *Arrows* point to the specks where active caspase-1 was concentrated. *E* and *F*, total fluorescence and number of specks per cell was measured from 10 imaging fields, respectively, from 10 imaging fields. *G*, apMIN6 cells were labeled with NHS before being added to HG-BMMs. *Scale bar*, 10 μm. *H*, HG-BMMs were incubated with NHS-apMIN6 cells and labeled with carboxy-H_2DFFDA to measure ROS and Hoechst to stain nuclei. *I*, BMMs kept in control or HG medium were cultured alone or overnight with apMIN6, and labeled with carboxy-H_2DFFDA and Hoechst. ROS was measured as carboxy-H_2DFFDA fluorescence per cell and normalized to that from control BMMs. $n = 12$ imaging fields. *Bar*, 20 μm. *, $p < 0.05$; **, $p < 0.01$; #, not significant by Student's *t* test. *J*, BMMs in control or HG medium were cultured overnight alone or with apMIN6 in the presence or absence of 10 mM trehalose or 0.5 mM NAC. Medium was collected after 24 h for ELISA of secreted IL-1β. *, $p < 0.05$ by ANOVA test.

longer had the elongated morphology (Fig. 8, *A* and *C*), which has been shown to indicate a transition to the proinflammatory phenotype (40). Transcription factor EB (TFEB) is a master regulator for many lysosomal and autophagy genes (41). TFEB was activated by β-cell efferocytosis, demonstrated by nuclear translocation of TFEB (Fig. 8*D*). As positive control, J7 cells were starved for 2 h to induce TFEB nuclear translocation (Fig. 8*D*). Efferocytosis of apMIN6 but not ap3T3-L1 cells induced long-term up-regulation of LAMP-1, a target of TFEB (Fig. 8*E*). The compensatory mechanism activated by lysosomal dysfunction (25) induced by β-cell efferocytosis would in turn promote macrophage inflammasome activation (9). Consistent with the finding that macrophages with active inflammasome complexes often undergo a form of cell death that is inherently

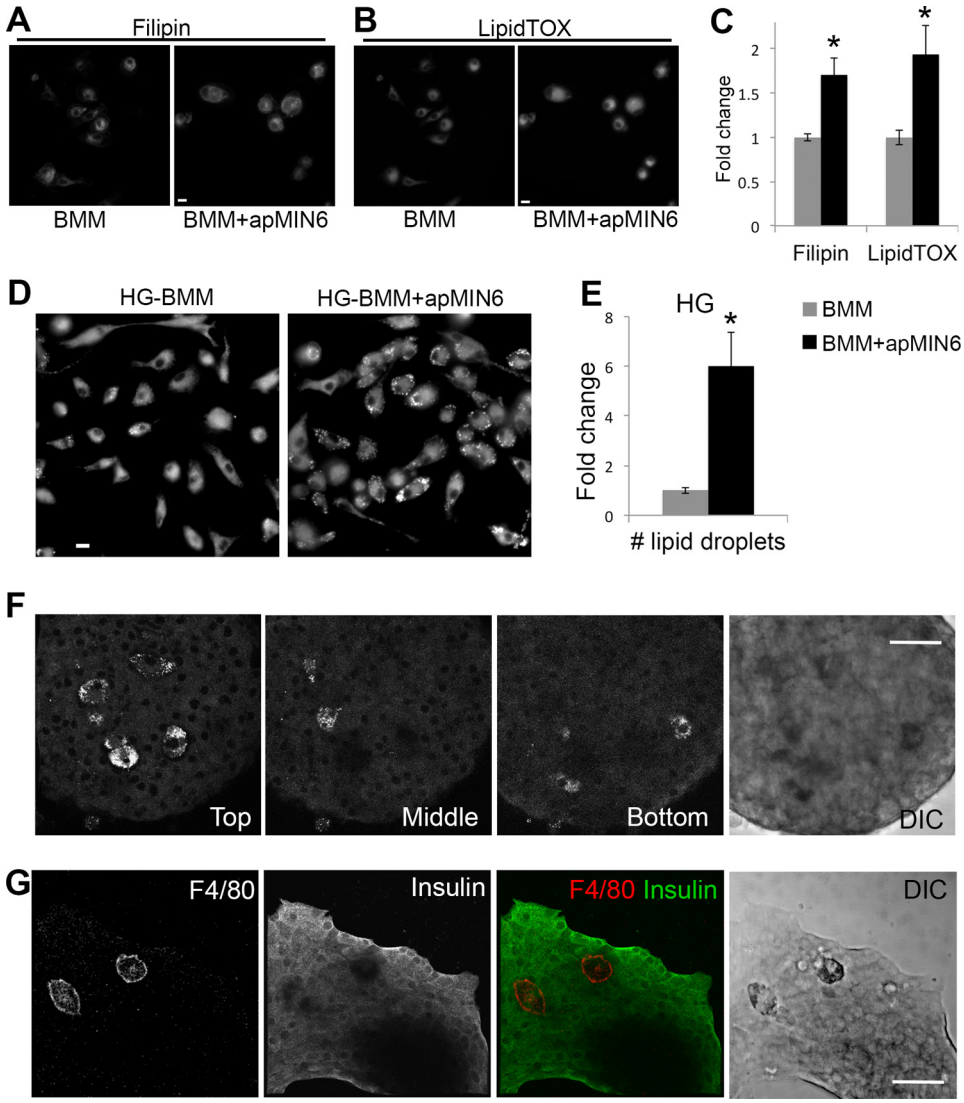

Figure 7. Lipid droplet formation in phagocytic HG-BMMs. *A–C,* BMMs cultured in normal growth medium showed increased cholesterol (labeled by filipin in *A*) and neutral lipid (labeled by LipidTOX in *B*) accumulation after β-cell efferocytosis. Total fluorescence intensity per cell was quantified in *C* from 10 imaging fields. *D* and *E,* BMMs cultured in HG medium showed increased lipid droplet formation (labeled by LipidTOX) after β-cell efferocytosis. Number of lipid droplets per cell was quantified in *E* from 9 imaging fields. *A–E, scale bars*, 10 μm; *, $p < 0.05$ *versus* BMM alone. *F,* isolated islets were cultured in HG, labeled with LipidTOX, and imaged by confocal microscopy. Three images of the same islet show islet macrophages present in different focal planes. *G,* isolated islets were cultured in HG, labeled with F4/80 and insulin antibodies, and imaged by confocal microscopy. *DIC*, differential interference contrast. *Scale bars*, 50 μm.

proinflammatory (42), we observed increased propidium iodide (PI) staining, a marker for cell death, specifically in phagocytic BMMs culture in HG (Fig. 8*F*).

Discussion

In this study, we show that phagocytosis of apoptotic β-cells by macrophages, a process that is significantly increased in T2DM, could contribute to islet dysfunction by macrophage proinflammatory reprogramming. Although there is abundant knowledge about the role of adipose tissue macrophages in T2DM, information on islet macrophages is critically lacking. By investigating how β-cell efferocytosis and elevated glucose work in synergy to impact macrophage function, we propose that the normally protective physiological process of apoptotic β-cell removal could generate destructive proinflammatory responses under diabetic conditions *in vitro*. Please note that this study was conducted entirely *in vitro* and validation of our findings *in vivo* is important in understanding how islet macrophages contribute to diabetes.

Many pathogenic crystals have been shown to induce lysosomal membrane permeabilization. However, they have only been studied in systems in which they were in direct contact with the macrophages. To our knowledge, this study is the first to examine the accumulation of crystals in the macrophage lysosomes by phagocytosis of apoptotic cells. Our data show insulin aggregates stayed in macrophage lysosomes for days after phagocytosis, indicating resistance to lysosomal degradation. This prompted us to test the idea that β-cell efferocytosis could activate the NLRP3 inflammasomes in macrophages via lysosomal destabilization, as do other nondegradable materials (17). Surprisingly, our results show that although accumulation of insulin crystals induced lysosomal swelling, it did not destabilize lysosomal membrane to the extent that caused significant

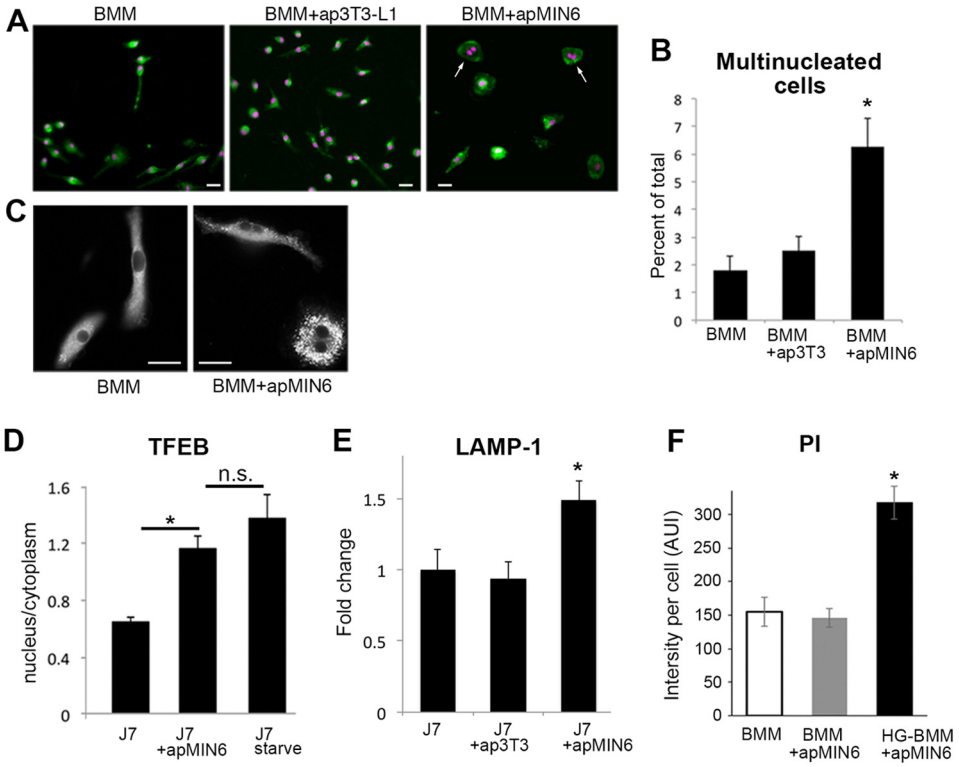

Figure 8. Phagocytosis of apMIN6 induces cellular changes associated with inflammation. *A* and *B,* BMMs, BMMs with ap3T3-L1, and BMMs with apMIN6 were labeled with CellTracker (*green*) and Hoechst (*purple*). *Bar*, 20 μm. The percent of multinucleated cells (*arrows*) was quantified from 9 imaging fields. *, $p < 0.05$ *versus* BMMs alone. *C,* HG-BMMs with or without β-cell efferocytosis were labeled with LipidTOX. *Bar*, 20 μm. *D,* J7 cells with or without β-cell efferocytosis were stained with TFEB antibody. TFEB translocation was measured by the ratio of TFEB fluorescence intensity in the nucleus to that in the cytoplasm. As positive control, cells were starved for 2 h to induce TFEB translocation. $n = 9$ imaging fields. *, $p < 0.05$ *versus* J7 alone. *n.s.*, not significant. *E,* total LAMP-1 fluorescence was quantified and normalized to cell area. Data are presented as fold-change relative to J7 cells alone. $n = 12$ imaging fields. *, $p < 0.05$ *versus* J7 alone. *F,* BMMs or HG-BMMs with or without β-cell efferocytosis were labeled with PI to measure cell death. $n = 9$ imaging fields. *, $p < 0.05$ *versus* BMMs alone.

lysosomal leakage. This might be because insulin crystals were much smaller in size compared with many of the established pathogenic crystal clusters. A more likely explanation may be that the anti-inflammatory nature of efferocytosis provided anti-oxidative measures to protect the macrophage lysosome (3, 43). On the other hand, when macrophages were exposed to high glucose, lysosomal leakage was clearly detected after β-cell efferocytosis. Similarly, we detected inflammasome activation, cytokine release, and lipid accumulation only when metabolic stress was present in addition to β-cell efferocytosis.

It has been suggested that the metabolic and inflammatory phenotypes of a macrophage are interdependent (44). Cholesterol crystals induce phagolysosomal damage and inflammasome activation, contributing to inflammation and atherosclerosis (9). It is unknown whether ingested insulin, by its crystalline nature, behaves similarly to cholesterol crystals in inducing inflammatory responses. Inflammatory activation from foam cells has been studied extensively yet almost exclusively in the context of atherosclerosis. Because lysosomal dysfunction inhibits cholesterol efflux (45), we showed formation of lipid-laden macrophage cells was induced by β-cell efferocytosis, but only under hyperglycemic conditions, suggesting that elevated glucose shifted β-cell efferocytosis from an anti-inflammatory to a pro-inflammatory mediator in macrophage polarization. This may contribute to the acceleration of atherogenesis in patients with T2DM (46).

ROS lies at the interface of metabolic and inflammatory pathways. Because all NLRP3-inflammasome activators examined to date trigger ROS generation, whereas ROS scavengers inhibit NLRP3 activation (34), it has been proposed that multiple activation pathways of NLRP3-inflammasomes converge on ROS signaling (47). Our data showed an increase in ROS production in BMMs after β-cell efferocytosis, especially with high glucose treatment. Among the various signals that activate NLRP3-inflammasomes, the lysosome rupture model is associated with pathogenic particulates (*e.g.* silica crystals, aluminum salts, and β-amyloid). Our data support lysosome leakage induced by β-cell efferocytosis in hyperglycemic macrophages.

This study shows that phagocytosis of apoptotic β-cells disrupts macrophage immune homeostasis, and that a diabetic milieu may tip the balance between pro- and anti-inflammatory responses. Slowly degradable insulin crystals can switch the anti-inflammatory action of efferocytosis to the pro-inflammatory action of inflammasome activation. This challenges our understanding of how apoptotic β-cells uniquely impact islet macrophage biology in the face of metabolic stress. Our results provide a new perspective on the causes of islet inflammation and highlight the importance of preserving macrophage lysosomal function as a therapeutic intervention for diabetes progression.

Experimental procedures

Cell culture

J774a.1 macrophage-like cells (American Type Culture Collection, Manassas, VA) were maintained in DMEM supplemented with 10% FBS, 50 units/ml of penicillin, and 50 μg/ml of streptomycin in a humidified, 5% CO_2 atmosphere at 37 °C. MIN6 cultured β-cells were grown in DMEM supplemented with 100 units/ml of penicillin, 100 μg/ml of streptomycin, 10% FBS, 2 mM L-glutamine, and 50 μM 2-mercaptoethanol. Mouse bone marrow macrophages were differentiated as previously described (48). Briefly, fibula and tibia bones were dissected from euthanized mice. The bone marrow was flushed using a 25-gauge needle and syringe under aseptic conditions. Bone marrow cells were incubated in DMEM supplemented with 10% heat-inactivated FBS and 20% L929-conditioned media. After 3 days, cell cultures were supplemented with an additional dose of L929-conditioned media (20% of volume). After 6 days of total culture, cells were visually inspected for attachment to untreated culture plates. For treatment with HG or HGP, DMEM containing 30 mM glucose or 30 mM glucose and 0.1 mM palmitate (49) was used after exposure to 11 mM glucose for 1 day. The control cells were kept in 11 mM glucose. The high glucose concentration does not represent a human physiologic condition; rather, it is a widely used tool in β-cell studies for glucotoxicity.

Materials and methods

Primary antibodies used were rabbit anti-LAMP-1 (Abcam), rat anti-F4/80 (Abd Serotec), guinea pig anti-insulin (Dako), and mouse anti-TFEB (Santa Cruz). LipidTOX, Alexa Fluor NHS Ester, cholera toxin subunit B Alexa Fluor 488, LysoTracker, CellTracker, DQ-ovalbumin, dextran conjugated to fluorescein and rhodamine, carboxy-H_2DFFDA, and all fluorescently labeled secondary antibodies were from Thermo Fisher Scientific. Collagenase P was from Roche Applied Science. IL-1β ELISA was from R and D systems (Minneapolis, MN). FAM FLICA activity assay was from Immunochemistry Technologies (Bloomington, MN). Hoechst 33342, Histopaque 1077 and 1119, and all other chemicals were from Sigma. KRBH buffer (128.8 mM NaCl, 4.8 mM KCl, 1.2 mM KH_2PO_4, 1.2 mM $MgSO_4$, 2.5 mM $CaCl_2$, 5 mM $NaHCO_3$, 10 mM HEPES, pH 7.4) was used for all experiments. Palmitate solution was prepared as described previously (49).

Islet isolation

Animal protocols were approved by the Institutional Animal Care and Use Committee at Weill Cornell Medical College. Islet isolation was performed with minor modifications (50). Collagenase P was first perfused through the common bile duct for digestion. Islets were separated from exocrine cells by gradient centrifugation using Histopaque 1077 and 1119, and further purified by manual picking.

Efferocytosis assay

Imaging of efferocytosis was carried out as described with modification (18). To induce apoptosis, MIN6 cells were irradiated with λ365 UV for 30 min, and then cultured for 16 h to allow apoptosis to develop. To induce islet apoptosis *in vivo*, ICR mice were injected intraperitoneally with 40 μg of STZ/g of body weight daily for 5 days to induce β-cell death (19). Two weeks after the last injection, islets were isolated, and seeded in imaging dishes overnight. To induce islet apoptosis *in vitro*, we cultured isolated islets with or without high glucose for 2 weeks. Apoptotic MIN6 (apMIN6) cells were incubated with J7 cells or BMMs at a ratio of 1:5 for 24 h, after which the co-culture was washed 4 times to remove floating cells. Imaging took place at the indicated time points after washing. To label with Alexa NHS dye, apMIN6 cells were incubated with Alexa Fluor NHS Ester diluted in 1 M NaOH, pH 9.0, for 2 h at 37 °C, 5% CO_2. After incubation, cells were washed 2 times to remove NaOH. CtB-Alexa Fluor 488 was used to label J7 cells on ice for 2 min followed by fixation for 15 min in 3% paraformaldehyde.

Fluorescence labeling

Cells were incubated with 500 nM LysoTracker or 10 μg/ml of DQ-ovalbumin for 30 min before imaging in KRBH buffer. For ROS, cells were incubated in 20 μM carboxy-H_2DFFDA for 1 h in culture media prior to imaging. Cells were washed and counterstained with Hoechst 33342 to quantify nuclei. Lysosomal pH was determined by FITC/rhodamine dextran as reported previously (27). To image dextran with antibody staining, BMMs were first cultured overnight alone or with apMIN6, then pulsed with 0.5 mg/ml of lysine-fixable tetramethylrhodamine-dextran for 16 h with a 4-h chase period, followed by fixation in 4% paraformaldehyde for 15 min, then blocking and permeabilization in 0.1% Tween 20 supplemented with 10% goat serum for 30 min. Cells were incubated with primary antibody for 1 h and with secondary antibody for 30 min, with the concentrations described below.

Immunofluorescence of islets containing BMMs

BMMs were identified by F4/80 or by preloaded dextran. Where dextran is shown, BMMs were first labeled with lysine-fixable dextran overnight and then added to islets in control or HG medium for 7 days. Islets containing BMMs were fixed in 3% paraformaldehyde for 1 h, permeabilized in 0.1% Triton X-100 for 30 min, and blocked with 10% goat serum in 0.2% Tween 20 for 1 h, all at room temperature. The following primary antibodies were used overnight at 4 °C: anti-F4/80 (1:100), anti-insulin (1:300), anti-LAMP-1 (1:125), and secondary antibody used at room temperature for 4 h at 1:400 with Alexa 546 anti-rat, Alexa 488 anti-guinea pig, and Alexa 633 anti-rabbit, respectively.

Fluorescence microscopy

Cells and islets were seeded in MatTek imaging dishes. Wide-field fluorescence microscopy utilized a Leica DMIRB microscope (Leica Mikroscopie und Systeme GmbH, Germany) equipped with a Princeton Instruments (Princeton, NJ) cooled charge coupled device using MetaMorph Imaging System software (Molecular Devices). Images were acquired at room temperature using an oil-immersion 40 × 1.25 NA oil-immersion objective. Hoechst and filipin images were captured using the UV filters. The green probes (DQ Ovalbu-

min, Alexa Fluor 488, LysoTracker, FITC, FAM FLICA, carboxy-H_2DFFDA, CellTracker) were imaged using a standard fluorescein filter cube (Chroma) on the wide-field microscope, and a 488–nm laser excitation with a 505–530–nm emission filter on the confocal microscope. The red probes (Alexa Fluor 546, Alexa Fluor 555, LipidTOX, tetramethylrhodamine, and DQ Ovalbumin excimers) were imaged using a standard rhodamine filter cube (Chroma) on the wide-field microscope, and a 543-nm laser excitation with a 560–615–nm emission filter on the confocal microscope. Alexa Fluor 633 was imaged using a standard Cy5 filter cube (Chroma) on the wide-field microscope and a 633–nm laser excitation with a 650–nm long pass emission filter on the confocal microscope. For confocal microscopy, the channels were scanned alternately with only one laser line and one detector channel on at a time. Images were corrected for background (51) and analyzed using MetaMorph software (Molecular Devices). Images were quantified either as individual cells or whole fields normalized to cell counts.

Gene expression

For quantitative RT-PCR, total RNA from macrophage cells was extracted from tissues using the Purelink® RNA kit. Total RNA (1 μg) was reverse transcribed using the SuperScript® Reverse Transcription system. Real-time PCR was performed on the cDNA on a Bio-Rad iCycler using SYBR Green master mix. All reagents were from Thermo Fisher Scientific. *Il1b* was expressed using *Gapdh* as reference: *Il1b* (forward, 5′-AAGGAGAACCAAGCAACGACAAAA-3′, reverse, TGGGGAACTCTGCAGACTCAAACT-3′); *Gapdh* (forward, 5′-ACTCCCACTCTTCCACCTTC-3′, reverse, 5′-TCTTGCTCAGTGTCCTTGC-3′).

Flow cytometry

UV-induced apMIN6 cells were stained with Alexa Fluor 647 NHS ester and added to J7 cells. After 24 h co-culture, the mixture was stained with cholera toxin subunit B conjugated with Alexa Fluor 488. Next, the cells were fixed and stained with insulin antibody and secondary antibody conjugated with Alexa Fluor 546. After staining, the cells were examined with flow cytometry (BD Fortessa). The gate was first set for cells double positive for Alexa 488 and Alexa 647. The selected population was analyzed for insulin staining by Alexa 546 intensity.

Statistical analysis

Unless otherwise indicated, each experiment was repeated three times. The number of cells or imaging fields used for quantification under each condition, *i.e.* the value of n used for statistical analysis, are listed in the figure legends. When individual lysosomes were quantified, the sample sizes were similar among groups, and the reported n refers to the smallest n used. Data are presented as the mean ± S.E. Statistical significance was analyzed using unpaired two-tailed Student's t tests for comparison between two groups and one-way repeated measures ANOVA with post hoc comparisons using the Tukey HSD test for data from more than two groups, with p values less than 0.05 deemed significant.

Author contributions—M. G. W. and M. H. conceptualization; M. G. W., G. L., and M. H. data curation; M. G. W., G. L., and M. H. formal analysis; M. G. W., G. L., and M. H. validation; M. G. W., G. L., and M. H. methodology; M. G. W. and M. H. writing-original draft; M. G. W. and M. H. writing-review and editing; M. H. supervision; M. H. funding acquisition; M. H. investigation; M. H. visualization; M. H. project administration.

Acknowledgments—We thank Drs. Abigail Haka, Valeria Barbosa-Lorenzi, and Rajesh Singh for helpful discussions and guidance on working with BMMs.

References

1. Donath, M. Y., and Shoelson, S. E. (2011) Type 2 diabetes as an inflammatory disease. *Nat. Rev. Immunol.* **11,** 98–107 CrossRef Medline
2. Green, D. R., Oguin, T. H., and Martinez, J. (2016) The clearance of dying cells: table for two. *Cell Death Differ.* **23,** 915–926 CrossRef Medline
3. Fadok, V. A., Bratton, D. L., Konowal, A., Freed, P. W., Westcott, J. Y., and Henson, P. M. (1998) Macrophages that have ingested apoptotic cells in vitro inhibit proinflammatory cytokine production through autocrine/paracrine mechanisms involving TGF-β, PGE2, and PAF. *J. Clin. Invest.* **101,** 890–898 CrossRef Medline
4. Halban, P. A. (1991) Structural domains and molecular lifestyles of insulin and its precursors in the pancreatic beta cell. *Diabetologia* **34,** 767–778 CrossRef Medline
5. Halban, P. A., Mutkoski, R., Dodson, G., and Orci, L. (1987) Resistance of the insulin crystal to lysosomal proteases: implications for pancreatic B-cell crinophagy. *Diabetologia* **30,** 348–353 CrossRef Medline
6. Howell, S. L. (1984) The mechanism of insulin secretion. *Diabetologia* **26,** 319–327 Medline
7. Martinon, F., Pétrilli, V., Mayor, A., Tardivel, A., and Tschopp, J. (2006) Gout-associated uric acid crystals activate the NALP3 inflammasome. *Nature* **440,** 237–241 CrossRef Medline
8. Prencipe, G., Caiello, I., Cherqui, S., Whisenant, T., Petrini, S., Emma, F., and De Benedetti, F. (2014) Inflammasome activation by cystine crystals: implications for the pathogenesis of cystinosis. *J. Am. Soc. Nephrol.* **25,** 1163–1169 CrossRef Medline
9. Duewell, P., Kono, H., Rayner, K. J., Sirois, C. M., Vladimer, G., Bauernfeind, F. G., Abela, G. S., Franchi, L., Nuñez, G., Schnurr, M., Espevik, T., Lien, E., Fitzgerald, K. A., Rock, K. L., Moore, K. J., *et al.* (2010) NLRP3 inflammasomes are required for atherogenesis and activated by cholesterol crystals. *Nature* **464,** 1357–1361 CrossRef Medline
10. Re, F. (2011) Inflammasome activation by pathogenic crystals and particles. In *The Inflammasomes* (Couillin I, Pétrilli V, and Martinon F, eds), 1st Ed., pp. 85–99, Springer Basel
11. Montgomery, R. R., Webster, P., and Mellman, I. (1991) Accumulation of indigestible substances reduces fusion competence of macrophage lysosomes. *J. Immunol.* **147,** 3087–3095 Medline
12. Ehses, J. A., Perren, A., Eppler, E., Ribaux, P., Pospisilik, J. A., Maor-Cahn, R., Gueripel, X., Ellingsgaard, H., Schneider, M. K., Biollaz, G., Fontana, A., Reinecke, M., Homo-Delarche, F., and Donath, M. Y. (2007) Increased number of islet-associated macrophages in type 2 diabetes. *Diabetes* **56,** 2356–2370 CrossRef Medline
13. Dinarello, C. A., Donath, M. Y., and Mandrup-Poulsen, T. (2010) Role of IL-1β in type 2 diabetes. *Curr. Opin. Endocrinol. Diabetes Obes.* **17,** 314–321 Medline
14. Youm, Y. H., Adijiang, A., Vandanmagsar, B., Burk, D., Ravussin, A., and Dixit, V. D. (2011) Elimination of the NLRP3-ASC inflammasome protects against chronic obesity-induced pancreatic damage. *Endocrinology* **152,** 4039–4045 CrossRef Medline
15. Westwell-Roper, C., Nackiewicz, D., Dan, M., and Ehses, J. A. (2014) Toll-like receptors and NLRP3 as central regulators of pancreatic islet inflammation in type 2 diabetes. *Immunol. Cell Biol.* **92,** 314–323 CrossRef Medline

16. Jourdan, T., Godlewski, G., Cinar, R., Bertola, A., Szanda, G., Liu, J., Tam, J., Han, T., Mukhopadhyay, B., Skarulis, M. C., Ju, C., Aouadi, M., Czech, M. P., and Kunos, G. (2013) Activation of the Nlrp3 inflammasome in infiltrating macrophages by endocannabinoids mediates beta cell loss in type 2 diabetes. *Nat. Med.* **19,** 1132–1140 CrossRef Medline
17. Masters, S. L., Dunne, A., Subramanian, S. L., Hull, R. L., Tannahill, G. M., Sharp, F. A., Becker, C., Franchi, L., Yoshihara, E., Chen, Z., Mullooly, N., Mielke, L. A., Harris, J., Coll, R. C., *et al.* (2010) Activation of the NLRP3 inflammasome by islet amyloid polypeptide provides a mechanism for enhanced IL-1β in type 2 diabetes. *Nat Immunol* **11,** 897–904 CrossRef Medline
18. Haka, A. S., Barbosa-Lorenzi, V. C., Lee, H. J., Falcone, D. J., Hudis, C. A., Dannenberg, A. J., and Maxfield, F. R. (2016) Exocytosis of macrophage lysosomes leads to digestion of apoptotic adipocytes and foam cell formation. *J. Lipid Res.* **57,** 980–992 CrossRef Medline
19. Szkudelski, T. (2001) The mechanism of alloxan and streptozotocin action in B cells of the rat pancreas. *Physiol. Res.* **50,** 537–546 Medline
20. Leenen, P. J., de Bruijn, M. F., Voerman, J. S., Campbell, P. A., and van Ewijk, W. (1994) Markers of mouse macrophage development detected by monoclonal antibodies. *J. Immunol. Methods* **174,** 5–19 CrossRef Medline
21. Cucak, H., Grunnet, L. G., and Rosendahl, A. (2014) Accumulation of M1-like macrophages in type 2 diabetic islets is followed by a systemic shift in macrophage polarization. *J. Leukoc. Biol.* **95,** 149–160 CrossRef Medline
22. Bidani, A., and Heming, T. A. (1995) Effects of bafilomycin A1 on functional capabilities of LPS-activated alveolar macrophages. *J. Leukoc. Biol.* **57,** 275–281 CrossRef Medline
23. Kuehnel, W. (2003) *Color Atlas of Cytology, Histology, & Microscopic Anatomy.* Thieme, New York
24. Orci, L., Ravazzola, M., Amherdt, M., Yanaihara, C., Yanaihara, N., Halban, P., Renold, A. E., and Perrelet, A. (1984) Insulin, not C-peptide (proinsulin), is present in crinophagic bodies of the pancreatic B-cell. *J. Cell Biol.* **98,** 222–228 CrossRef Medline
25. Emanuel, R., Sergin, I., Bhattacharya, S., Turner, J., Epelman, S., Settembre, C., Diwan, A., Ballabio, A., and Razani, B. (2014) Induction of lysosomal biogenesis in atherosclerotic macrophages can rescue lipid-induced lysosomal dysfunction and downstream sequelae. *Arterioscler. Thromb. Vasc. Biol.* **34,** 1942–1952 CrossRef Medline
26. Diwu, Z., Chen, C. S., Zhang, C., Klaubert, D. H., Haugland, R. P. (1999) A novel acidotropic pH indicator and its potential application in labeling acidic organelles of live cells. *Chem. Biol.* **6,** 411–418 CrossRef Medline
27. Dunn, K., and Maxfield, F. R. (2003) Ratio imaging instrumentation. *Methods Cell Biol.* **72,** 389–413 CrossRef Medline
28. Santambrogio, L., Sato, A. K., Carven, G. J., Belyanskaya, S. L., Strominger, J. L., and Stern, L. J. (1999) Extracellular antigen processing and presentation by immature dendritic cells. *Proc. Natl. Acad. Sci. U.S.A.* **96,** 15056–15061 CrossRef Medline
29. Song, A., Zhu, L., Gorantla, G., Berdysz, O., Amici, S. A., Guerau-de-Arellano, M., Madalena, K. M., Lerch, J. K., Liu, X., and Quan, N. (2018) Salient type 1 interleukin 1 receptor expression in peripheral non-immune cells. *Sci. Rep.* **8,** 723 CrossRef Medline
30. Böni-Schnetzler, M., Boller, S., Debray, S., Bouzakri, K., Meier, D. T., Prazak, R., Kerr-Conte, J., Pattou, F., Ehses, J. A., Schuit, F. C., and Donath, M. Y. (2009) Free fatty acids induce a proinflammatory response in islets via the abundantly expressed interleukin-1 receptor I. *Endocrinology* **150,** 5218–5229 CrossRef Medline
31. Zhang, X., Dai, J., Li, L., Chen, H., and Chai, Y. (2017) NLRP3 inflammasome expression and signaling in human diabetic wounds and in high glucose induced macrophages. *J. Diabetes Res.* **2017,** 5281358 Medline
32. Van Opdenbosch, N., Gurung, P., Vande Walle, L., Fossoul, A., Kanneganti, T. D., and Lamkanfi, M. (2014) Activation of the NLRP1b inflammasome independently of ASC-mediated caspase-1 autoproteolysis and speck formation. *Nat. Commun.* **5,** 3209 CrossRef Medline
33. Shi, C. S., Shenderov, K., Huang, N. N., Kabat, J., Abu-Asab, M., Fitzgerald, K. A., Sher, A., and Kehrl, J. H. (2012) Activation of autophagy by inflammatory signals limits IL-1beta production by targeting ubiquitinated inflammasomes for destruction. *Nat. Immunol.* **13,** 255–263 CrossRef Medline
34. Dostert, C., Pétrilli, V., Van Bruggen, R., Steele, C., Mossman, B. T., and Tschopp, J. (2008) Innate immune activation through Nalp3 inflammasome sensing of asbestos and silica. *Science* **320,** 674–677 CrossRef Medline
35. Zawada, A. M., Rogacev, K. S., Rotter, B., Winter, P., Marell, R. R., Fliser, D., and Heine, G. H. (2011) SuperSAGE evidence for CD14++CD16+ monocytes as a third monocyte subset. *Blood* **118,** e50–61 CrossRef Medline
36. Sergin, I., Evans, T. D., Zhang, X., Bhattacharya, S., Stokes, C. J., Song, E., Ali, S., Dehestani, B., Holloway, K. B., Micevych, P. S., Javaheri, A., Crowley, J. R., Ballabio, A., Schilling, J. D., Epelman, S., *et al.* (2017) Exploiting macrophage autophagy-lysosomal biogenesis as a therapy for atherosclerosis. *Nat. Commun.* **8,** 15750 CrossRef Medline
37. Helming, L., and Gordon, S. (2009) Molecular mediators of macrophage fusion. *Trends Cell Biol.* **19,** 514–522 CrossRef Medline
38. MacLauchlan, S., Skokos, E. A., Meznarich, N., Zhu, D. H., Raoof, S., Shipley, J. M., Senior, R. M., Bornstein, P., and Kyriakides, T. R. (2009) Macrophage fusion, giant cell formation, and the foreign body response require matrix metalloproteinase 9. *J. Leukoc. Biol.* **85,** 617–626 CrossRef Medline
39. Brodbeck, W. G., and Anderson, J. M. (2009) Giant cell formation and function. *Curr. Opin. Hematol.* **16,** 53–57 CrossRef Medline
40. McWhorter, F. Y., Wang, T., Nguyen, P., Chung, T., and Liu, W. F. (2013) Modulation of macrophage phenotype by cell shape. *Proc. Natl. Acad. Sci. U.S.A.* **110,** 17253–17258 CrossRef Medline
41. Settembre, C., Di Malta, C., Polito, V. A., Garcia Arencibia, M., Vetrini, F., Erdin, S., Erdin, S. U., Huynh, T., Medina, D., Colella, P., Sardiello, M., Rubinsztein, D. C., and Ballabio, A. (2011) TFEB links autophagy to lysosomal biogenesis. *Science* **332,** 1429–1433 CrossRef Medline
42. Fink, S. L., and Cookson, B. T. (2006) Caspase-1-dependent pore formation during pyroptosis leads to osmotic lysis of infected host macrophages. *Cell Microbiol.* **8,** 1812–1825 CrossRef Medline
43. Korns, D., Frasch, S. C., Fernandez-Boyanapalli, R., Henson, P. M., and Bratton, D. L. (2011) Modulation of macrophage efferocytosis in inflammation. *Front. Immunol.* **2,** 57 Medline
44. Tabas, I., and Bornfeldt, K. E. (2016) Macrophage phenotype and function in different stages of atherosclerosis. *Circ. Res.* **118,** 653–667 CrossRef Medline
45. Ouimet, M., Franklin, V., Mak, E., Liao, X., Tabas, I., and Marcel, Y. L. (2011) Autophagy regulates cholesterol efflux from macrophage foam cells via lysosomal acid lipase. *Cell Metab* **13,** 655–667 CrossRef Medline
46. Silva, J. A., Escobar, A., Collins, T. J., Ramee, S. R., and White, C. J. (1995) Unstable angina: a comparison of angioscopic findings between diabetic and nondiabetic patients. *Circulation* **92,** 1731–1736 CrossRef Medline
47. Tschopp, J., and Schroder, K. (2010) NLRP3 inflammasome activation: the convergence of multiple signalling pathways on ROS production? *Nat. Rev. Immunol.* **10,** 210–215 CrossRef Medline
48. Weischenfeldt, J., and Porse, B. (2008) Bone marrow-derived macrophages (BMM): isolation and applications. *CSH Protoc.* **2008,** pdb prot5080 Medline
49. Cousin, S. P., Hügl, S. R., Wrede, C. E., Kajio, H., Myers, M. G., Jr., and Rhodes, C. J. (2001) Free fatty acid-induced inhibition of glucose and insulin-like growth factor I-induced deoxyribonucleic acid synthesis in the pancreatic beta-cell line INS-1. *Endocrinology* **142,** 229–240 CrossRef Medline
50. Carter, J. D., Dula, S. B., Corbin, K. L., Wu, R., and Nunemaker, C. S. (2009) A practical guide to rodent islet isolation and assessment. *Biol. Proced. Online* **11,** 3–31 CrossRef Medline
51. Hao, M., and Maxfield, F. R. (2000) Characterization of rapid membrane internalization and recycling. *J. Biol. Chem.* **275,** 15279–15286 CrossRef Medline